Target Cell–Dependent Normalization of Transmitter Release at Neocortical Synapses

Helmut J. Koester[1,2*†] and Daniel Johnston[2*]

The efficacy and short-term modification of neocortical synaptic connections vary with the type of target neuron. We investigated presynaptic Ca^{2+} and release probability at single synaptic contacts between pairs of neurons in layer 2/3 of the rat neocortex. The amplitude of Ca^{2+} signals in boutons of pyramids contacting bitufted or multipolar interneurons or other pyramids was dependent on the target cell type. Optical quantal analysis at single synaptic contacts suggested that release probabilities are also target cell–specific. Both the Ca^{2+} signal and the release probability of different boutons of a pyramid contacting the same target cell varied little. We propose that the mechanisms that regulate the functional properties of boutons of a pyramid normalize the presynaptic Ca^{2+} influx and release probability for all those boutons that innervate the same target cell.

Synapses are believed to be important sites for learning and memory. Synapses between neurons are heterogeneous in synaptic efficacy and show distinct forms of short-term plasticity. One determinant of synaptic efficacy and short-term plasticity is the probability of neurotransmitter release. The rate and type of information transfer across a synapse are dependent on release probability and short-term plasticity (*1*, *2*). Furthermore, the computational function of neurons within a network depends on the form of short-term plasticity of the synapses they receive (*3*, *4*). Release probability has not been directly determined in synaptic connections in situ, only for autapses in tissue culture (*5*). The small size of synapses, their electrotonic isolation from somata, and the high density of cellular structures in brain tissue has prevented the direct measurement of release probability among synapses of connected pairs of neocortical neurons.

Synaptic connections between pyramids and interneurons in layer 2/3 (L2/3) of the somatosensory cortex of young rats have different efficacy, reliability, and short-term plasticity (*6*–*8*). These differences may depend on presynaptic factors such as influx of calcium ions (Ca^{2+}), Ca^{2+} buffering and diffusion in the cytoplasm, the Ca^{2+} sensor for release, and Ca^{2+} extrusion (*8*–*10*). Consistent with this view, the boutons of pyramid axons in L2/3 show a relatively wide range of action potential (AP)–evoked Ca^{2+} signal amplitudes, varying up to 10-fold between different boutons of the same axonal arbor (*11*–*13*). A synaptic connection between neocortical cells is, in most cases, formed by several synaptic contacts (*14*–*17*), and their individual properties are unknown.

To elucidate how a single contact contributes to the net behavior of a synaptic connection between two neurons and to examine presynaptic determinants of target-cell specificity, we used high-resolution fluorescence imaging (*18*–*20*) to examine pre- or postsynaptic AP-evoked Ca^{2+} transients in 63 single synaptic contacts. Synaptically connected pairs of neurons in L2/3 of the somatosensory neocortex of young rats were examined in acute brain slices by dual whole-cell voltage recordings under visual control (*21*, *22*). Pre- and postsynaptic cells of a pair were classified based on discharge pattern and dendritic morphology (*6*, *7*). To examine Ca^{2+} signals of pyramidal cell boutons contacting different target cells, we loaded presynaptic pyramids with Oregon Green 488 Bapta-1 (OGB-1, 200 μM) and postsynaptic neurons with Alexa 594 (Fig. 1A). Contacts were identified by (i) the overlap of an axon of the presynaptic pyramid and a dendrite of the postsynaptic cell, and (ii) the presence of an axonal varicosity where axons and dendrites were apposed (Fig. 1B). The fact that, in most cases, appositions selected in this way were indeed functional synaptic contacts was verified by postsynaptic Ca^{2+} imaging (see below).

Pyramid-to-bitufted (P-B) connections (Fig. 1) formed mostly axospinous contacts (>60%). We examined those bitufted interneurons that showed frequency adaptation of APs and facilitation of excitatory postsynaptic potentials (EPSPs) in response to evoked APs in the presynaptic pyramid. These connections had low efficacy and high failure rates and showed paired-pulse facilitation (Fig. 1C and Table 1).

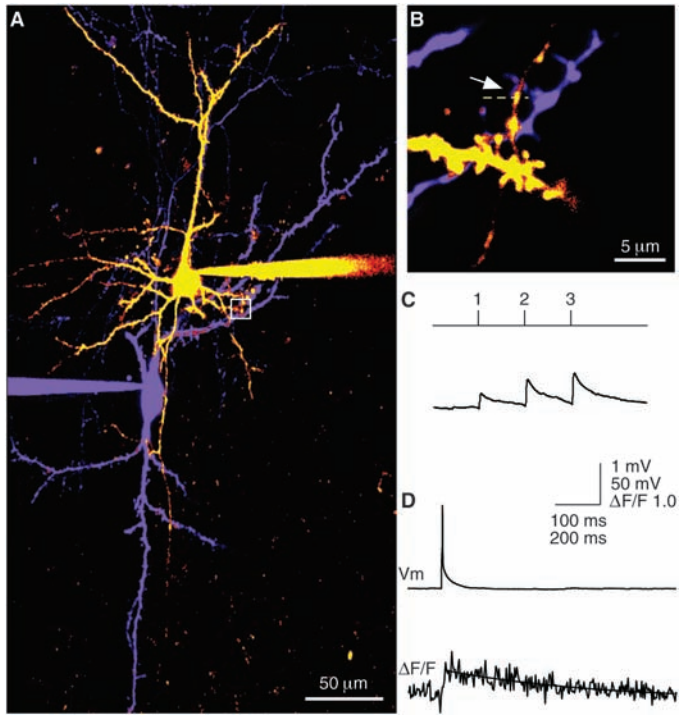

Fig. 1. Identification of single synaptic contacts in P-B connections. (**A**) Overlay of an L2/3 pyramidal neuron filled with OGB-1 (yellow, pseudocolor) and a bitufted interneuron filled with Alexa 594 (blue, pseudocolor). Recording pipettes are attached to somata. The white square indicates the location of the synaptic contact in (B). (**B**) A synaptic contact (arrow) examined for presynaptic Ca^{2+} signals in response to presynaptic APs. The broken yellow line indicates the position of the line scan. (**C**) A train of APs (three APs at 10 Hz), evoked by brief current injections in the presynaptic pyramidal cell, elicited EPSPs in the postsynaptic interneuron (lower trace, average of 20 sweeps) that successively increased in amplitude. (**D**) An AP in the presynaptic pyramid (upper trace) evoked a small Ca^{2+} fluorescence signal (lower trace) in the bouton at the synaptic contact illustrated in (B). The continuous line represents a single exponential fit. The Ca^{2+} signals shown do not reflect the physiological amplitude and time course of $[Ca^{2+}]_i$ in a bouton, because the indicator OGB-1 acts as an exogenous Ca^{2+} buffer (*28*, *29*).

[1]Abteilung Zellphysiologie, Max-Planck-Institut für Medizinische Forschung, Jahnstraße 29, D-69120 Heidelberg, Germany. [2]Department of Neuroscience, Baylor College of Medicine, One Baylor Plaza, Houston, TX 77030, USA.

*Present address: Center for Learning and Memory, University of Texas at Austin, Austin, TX 78712, USA. †To whom correspondence should be addressed. E-mail: HKoester@mail.utexas.edu

Ca^{2+} signals in boutons of contacts of these connections, evoked by a single presynaptic AP, were small [relative calcium fluorescence change $\Delta F/F = 0.54 \pm 0.29$, mean ± SD (*22*), $n = 12$ boutons] (Fig. 1D) compared to the average AP-evoked Ca^{2+} signal in pyramidal cell boutons measured under the same conditions [$\Delta F/F = 1.31 \pm 0.68$ (*12*)]. Pyramid-to-multipolar (P-M) connections had different characteristics (Fig. 2). Contacts were mostly axodendritic (>80%) and located close to the (postsynaptic) soma; the failure rate was low; synaptic efficacy was high; and evoked EPSPs showed paired-pulse depression (Fig. 2C and Table 1). AP-evoked presynaptic Ca^{2+} signals had an average amplitude of $\Delta F/F = 1.62 \pm 0.43$ ($n = 11$ boutons), about threefold as large as that measured in boutons of P-B connections. This difference was significant [$P < 0.01$, analysis of variance (ANOVA)]. Finally, pyramid-to-pyramid (P-P) connections also had low failure rates (Table 1). P-P connections usually showed depression and only in a few cases (15%) displayed paired-pulse facilitation. P-P contacts were mostly axospinous (>60%). Presynaptic $[Ca^{2+}]_i$ (intracellular calcium concentration) transients ranged from $\Delta F/F = 0.25$ to 2.28; the average amplitude was $\Delta F/F = 0.96 \pm 0.67$ ($n = 8$ boutons, $P < 0.05$ compared to P-M connections, ANOVA). We did not find significant differences in the presynaptic Ca^{2+} signal between axospinous and axodendritic contacts for any of the three classes of connections between pyramids and different target cell types ($P > 0.05$, t tests). The low z-resolution did not allow us to identify spines reliably in all cases, and thus the number of axospinous contacts is underestimated. Connections with larger presynaptic Ca^{2+} signals had a lower EPSP failure rate (Fig. 2E).

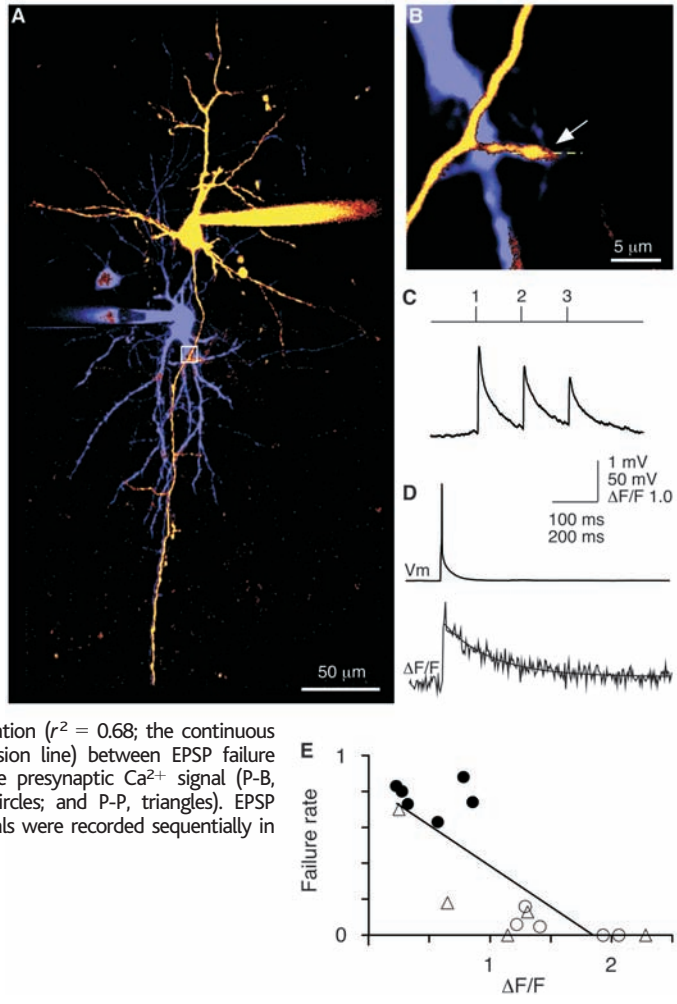

Fig. 2. Identification of single synaptic contacts in P-M connections. (**A**) Overlay of an L2/3 pyramidal neuron filled with OGB-1 (yellow, pseudocolor) and a multipolar interneuron filled with Alexa 594 (blue, pseudocolor). (**B**) A synaptic contact examined for a presynaptic Ca^{2+} signal in response to a presynaptic AP. The broken yellow line indicates the position of the line scan. (**C**) A presynaptic train of APs (three APs at 10 Hz) elicited EPSPs in the postsynaptic multipolar interneuron (lower trace, average of 20 sweeps) that decreased in amplitude. (**D**) An AP in the presynaptic pyramid (upper trace) evoked a large Ca^{2+} fluorescence signal in the bouton at the synaptic contact illustrated in (B). (**E**) Graph of the linear correlation ($r^2 = 0.68$; the continuous line represents the regression line) between EPSP failure rate and amplitude of the presynaptic Ca^{2+} signal (P-B, solid circles; P-M, open circles; and P-P, triangles). EPSP failure rate and Ca^{2+} signals were recorded sequentially in each pair.

The three classes of connections not only differ in reliability but also in frequency-dependent short-term plasticity. The presynaptic Ca^{2+} fluorescence transients evoked by a single AP and by trains of three APs (at 10 Hz) in P-B connections had similar amplitudes. The amplitude ratios of the second and third Ca^{2+} transient to the first were, on average, 96 ± 42% and 103 ± 24% [$n = 7$ boutons], respectively. In contrast, in P-M connections, the second and third APs evoked a fluorescence signal with peak amplitudes of 94 ± 17% and 83 ± 23% ($n = 9$ boutons), compared to the first AP. In P-P connections, the second and third amplitudes were 97 ± 28% and 84 ± 24% ($n = 4$ boutons). This decrease in amplitude for P-M and P-P connections, however, is presumably due to saturation of the high-affinity Ca^{2+} indicator OGB-1. This was indicated by the inverse correlation of the relative amplitude of the third response with the amplitude of the first ($r^2 = 0.48$ and $r^2 = 0.61$). Furthermore, in experiments with a low-affinity indicator in single-cell recordings, summation was always linear (*12*).

When we examined two or more synaptic contacts of the same connection, the variability in the amplitude of the Ca^{2+} signals between boutons was very small. The high correlation ($r^2 = 0.78$) of amplitudes measured in different boutons of the same connection indicated that the variability between boutons of a pair was small (Fig. 4C). Assuming that the volume-averaged Ca^{2+} signals were proportional to the initial fast Ca^{2+} influx that briefly increases the transmitter release probability (*23*), the small difference between different boutons of a particular connection suggested that the increase in release probability, evoked by a single AP, could be comparable for all release sites.

We tested this hypothesis in a second series of experiments by optical quantal analysis. Postsynaptic cells were filled with the Ca^{2+} indicator (OGB-1, 100 μM), and Alexa 594 was loaded into the presynaptic pyramid (Fig. 3). Potential synaptic contacts (Fig. 3B) were

Table 1. Properties of L2/3 synaptic connections. The table shows average values and the number of recordings (n) for connections between pyramids and various target cell types. The paired-pulse ratio was measured at 10 Hz from the ratio of the first and second peaks in a train of three APs. Pre- and postsynaptic distance refer to the geometric distance in xy (neglecting z) of a synaptic contact from pre- and postsynaptic soma.

Synapse property	Target cell type		
	L2/3 pyramid (n)	Multipolar (n)	Bitufted (n)
Unitary EPSP (mV)	0.92 ± 1.01 (34)	2.35 ± 1.40 (8)	0.22 ± 0.19 (22)
Failure rate (%)	22 ± 21 (34)	4 ± 6 (8)	69 ± 19 (22)
Paired-pulse ratio (%)	77 ± 35 (26)	66 ± 9 (8)	223 ± 126 (18)
Postsynaptic distance (μm)	55 ± 30 (21)	38 ± 37 (14)	89 ± 78 (23)
Presynaptic $\Delta F/F$	0.96 ± 0.67 (8)	1.62 ± 0.43 (11)	0.54 ± 0.29 (12)
Release probability/contact	0.46 ± 0.26 (17)	0.64 ± 0.16 (3)	0.13 ± 0.08 (12)

examined for a postsynaptic Ca^{2+} signal in response to a presynaptic AP (Fig. 3D). These fluorescence signals were a result of postsynaptic Ca^{2+} influx, presumably mediated by *N*-methyl-D-aspartate receptors (*20*, *24*). The Ca^{2+} signals were highly localized, and their occurrence varied stochastically, indicating successes and failures of presynaptic APs to elicit transmitter release (Fig. 3E). The optically measured release probability, p_r, ranged from 0.05 to 0.92 and was dependent on target cell type. Average postsynaptic resting membrane voltages in these experiments were –63 mV (P-B), –66 mV (P-M), and –67 mV (P-P). In P-B connections ($p_r = 0.13 \pm 0.08$, $n = 12$ contacts), release probability was significantly lower than in P-M connections ($p_r = 0.64 \pm 0.16$, $n = 3$ contacts, $P < 0.01$, ANOVA) or in P-P connections ($p_r = 0.46 \pm 0.26$, $n = 17$ contacts, $P < 0.01$, ANOVA). These differences suggest that, in addition to the target-cell specificity of Ca^{2+} transients, the release probability of individual pyramidal cell boutons was also target cell–dependent (Fig. 4). In agreement with the presynaptic Ca^{2+} signal measurements, we found no significant difference in release probability for axospinous and axodendritic contacts in the three classes of connections ($P > 0.05$, *t* tests).

When two synaptic contacts of the same connection were examined, their release probabilities were similar (Fig. 4D) ($n = 15$ pairs of contacts). The individual contacts were usually located on different branches of the dendritic and axonal arbors and thus were presumably independent. In no pair of contacts did we find a significant difference in release probability [tested with χ^2-statistics ($P < 0.05$) or by Fisher's exact probability test (for small release probabilities)]. We refer to this as normalization of release probability for different boutons of a connection. It was independent of the distance of contacts to each other (Fig. 4E). The release probabilities of two contacts of a connection were correlated for P-B connections ($r^2 = 0.77$) and for P-P connections ($r^2 = 0.91$).

Simulations of binomial and intersite variation showed that the distributions of release probabilities are consistent with a coefficient of variation of 0.16 for P-B and 0.19 for P-P connections (*22*). The experimental and simulation results indicate a small width for the distribution of release probabilities for all contacts within a given connection. These results suggest a model for neocortical synaptic connections that assumes binomial release, similar release probabilities, and varying quantal contents for the release sites. We tested a simple version of this model (the normalization model, assuming zero intersite variability in p_r) to see if it is consistent with the observed EPSP amplitude distributions. Using standard hypothesis testing (*25*, *26*), we could reject simple and compound binomial models underlying EPSP amplitude distributions in ~50% of the experiments, in favor of the normalization model (*22*).

The results document a target cell–specific difference of volume-averaged Ca^{2+} signals evoked by an AP in single boutons of L2/3 pyramidal cells. The size of the Ca^{2+} signal is substantially larger in connections with higher efficacy and reliability. A comparable target-cell specificity was found for optically measured release probabilities at individual synaptic contacts. Thus, both Ca^{2+} inflow and release probability of a bouton are target cell–specific. Target-cell specificity might be even more stringent than reported here, because interneuron classes, as defined by the AP discharge pattern and dendritic/axonal morphology, may represent an inhomogeneous cell population (*27*). Furthermore, the results are biased for those contacts that are located close (on average within <100 μm) to somata of both pre- and postsynaptic neurons, as a result of our searching procedure for contacts along the axon. Whether the difference between Ca^{2+} signals in boutons innervating different classes of target cells is a result of differences in Ca^{2+} channel density or channel subtypes, the endogenous Ca^{2+} buffer ratio, the size of these boutons, or a combination of these factors cannot be determined at present.

Different boutons of an individual connection had Ca^{2+} transients of similar amplitude, even if the boutons were located as far as 300 μm apart. This normalization of synaptic contacts of a connection was unexpected, because there is no obvious postsynaptic signal known at present that would operate over such large distances. Different boutons of a pyramid have a wide range of Ca^{2+} amplitudes even for nearby boutons of the same axon branch (*11*, *12*). In accordance with the idea of a normalization of presynaptic Ca^{2+} transients, we also found a normalization of release probabilities for different contacts of a connection. This suggests that one factor contributing to the normalization of release in all boutons of a layer 2/3 pyramidal cell that contact the same target cell is the size of the presynaptic Ca^{2+} influx. The normalization might be simply a result of target-cell specificity. However, there is no indication of such a fine subclassification of neurons.

We are therefore left with the conclusion that the normalization could arise from the unique pattern of pre- and postsynaptic activity that is similar for all contacts of a given

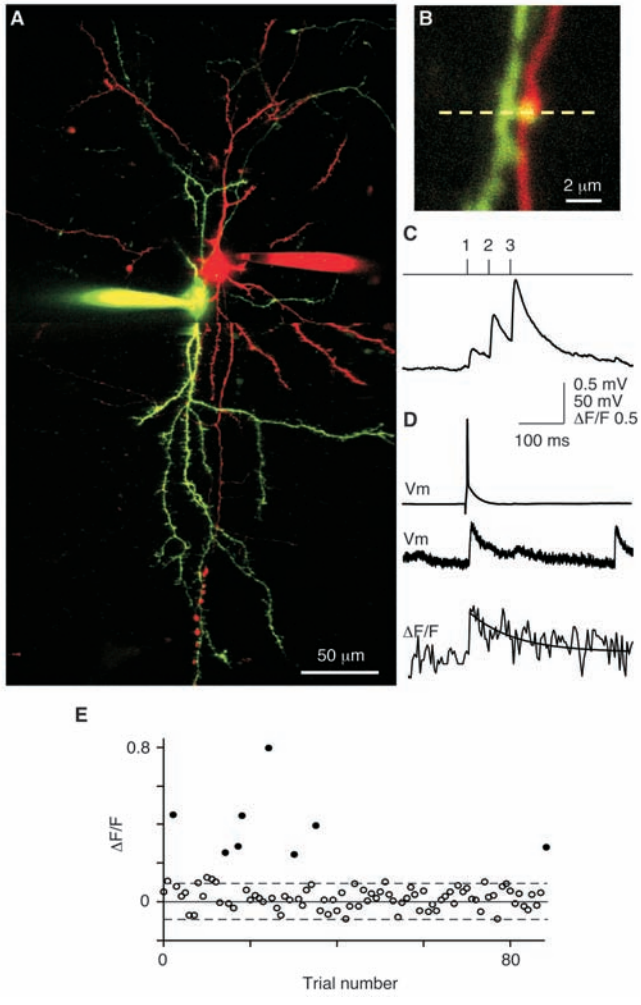

Fig. 3. Optical quantal analysis in a P-B cell connection. (**A**) Overlay of an L2/3 presynaptic pyramid filled with Alexa 594 (red, pseudocolor) and a postsynaptic bitufted neuron filled with OGB-1 (green, pseudocolor). The resting membrane voltage of the bitufted neuron was –59 mV. (**B**) Fluorescence image of a synaptic contact. The broken yellow line indicates the scan line. (**C**) Presynaptic stimulation of APs at 20 Hz (indicated by numbers) evoked facilitating EPSPs in the bitufted cell (average of 50 sweeps). (**D**) A single presynaptic AP (upper trace) evoked an EPSP in the postsynaptic cell (middle trace) and a Ca^{2+} fluorescence transient (lower trace) in the spine shown in (B). The continuous line represents a single-exponential fit to the data. (**E**) The graph shows the amplitude of the Ca^{2+} fluorescence signal ($\Delta F/F$) of all recordings in the spine shown in (B). Successes of transmission (solid circles) were easily distinguished from failures (open circles). Broken lines approximate the noise of the recordings.

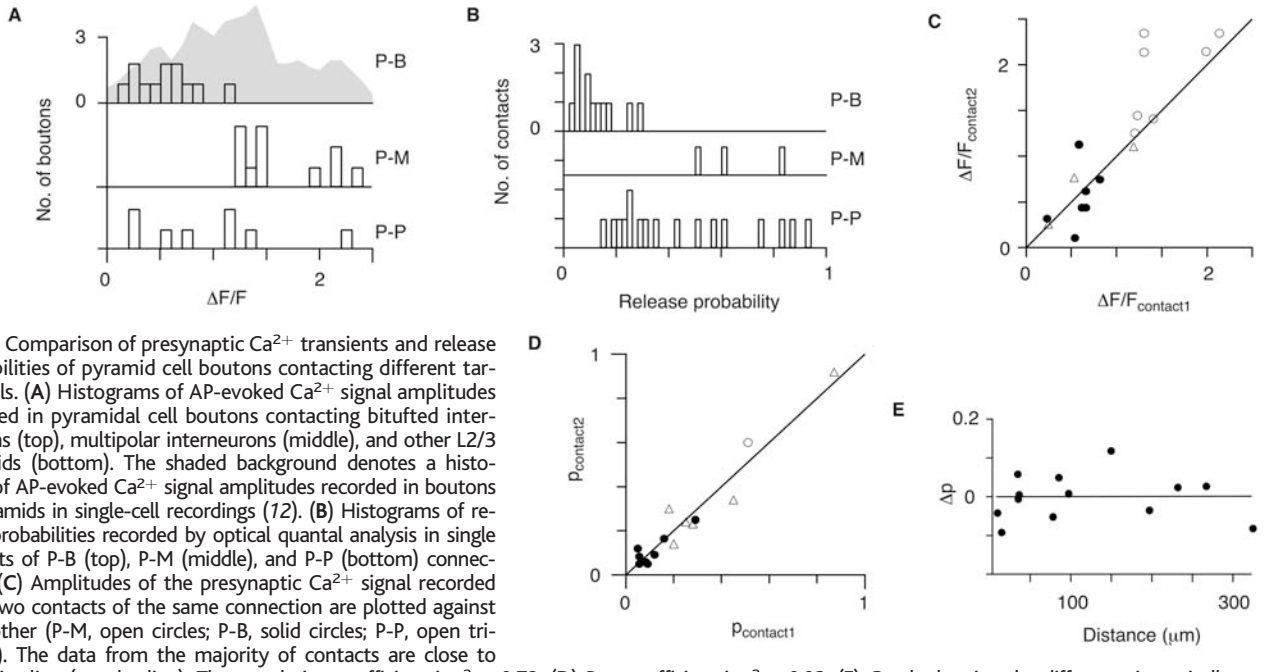

Fig. 4. Comparison of presynaptic Ca^{2+} transients and release probabilities of pyramid cell boutons contacting different target cells. (**A**) Histograms of AP-evoked Ca^{2+} signal amplitudes recorded in pyramidal cell boutons contacting bitufted interneurons (top), multipolar interneurons (middle), and other L2/3 pyramids (bottom). The shaded background denotes a histogram of AP-evoked Ca^{2+} signal amplitudes recorded in boutons of pyramids in single-cell recordings (*12*). (**B**) Histograms of release probabilities recorded by optical quantal analysis in single contacts of P-B (top), P-M (middle), and P-P (bottom) connections. (**C**) Amplitudes of the presynaptic Ca^{2+} signal recorded from two contacts of the same connection are plotted against each other (P-M, open circles; P-B, solid circles; P-P, open triangles). The data from the majority of contacts are close to the unity line (angular line). The correlation coefficient is $r^2 = 0.78$. (**D**) Release probability p_r recorded in one contact plotted against another contact of the same connection (P-M, open circles; P-B, solid circles; P-P, open triangles). All data points are close to the unity line (angular line). The correlation coefficient is $r^2 = 0.93$. (**E**) Graph showing the difference in optically measured release probability of two contacts of a connection plotted against the geometric distance of the two contacts. There is no correlation between these two parameters ($r^2 = 3 \times 10^{-5}$). The continuous line represents the regression line.

connection. Finally, the fact that P-P connections have the largest variability in their release probability may suggest that they can be more readily changed in the long term, for example as a function of usage.

References and Notes

1. A. Zador, *J. Neurophysiol.* **79**, 1219 (1998).
2. H. Markram, A. Gupta, A. Uziel, Y. Wang, M. Tsodyks, *Neurobiol. Learn. Mem.* **70**, 101 (1998).
3. D. L. Cook, P. C. Schwindt, L. A. Grande, W. J. Spain, *Nature* **421**, 66 (2003).
4. L. F. Abbott, J. A. Varela, K. Sen, S. B. Nelson, *Science* **275**, 220 (1997).
5. V. N. Murthy, T. J. Sejnowski, C. F. Stevens, *Neuron* **18**, 599 (1997).
6. A. Reyes *et al.*, *Nat. Neurosci.* **1**, 279 (1998).
7. H. Markram, Y. Wang, M. Tsodyks, *Proc. Natl. Acad. Sci. U.S.A.* **95**, 5323 (1998).
8. A. Rozov, N. Burnashev, B. Sakmann, E. Neher, *J. Physiol.* **531**, 807 (2001).
9. J. H. Bollmann, B. Sakmann, J. G. Borst, *Science* **289**, 953 (2000).
10. R. Schneggenburger, E. Neher, *Nature* **406**, 889 (2000).
11. C. L. Cox, W. Denk, D. W. Tank, K. Svoboda, *Proc. Natl. Acad. Sci. U.S.A.* **97**, 9724 (2000).
12. H. J. Koester, B. Sakmann, *J. Physiol.* **529**, 625 (2000).
13. I. Llano, Y. P. Tan, C. Caputo, *J. Physiol.* **502**, 509 (1997).
14. D. Feldmeyer, V. Egger, J. Lubke, B. Sakmann, *J. Physiol.* **521**, 169 (1999).
15. N. Toni, P. A. Buchs, I. Nikonenko, C. R. Bron, D. Muller, *Nature* **402**, 421 (1999).
16. E. H. Buhl *et al.*, *J. Physiol.* **500**, 689 (1997).
17. H. Markram, J. Lubke, M. Frotscher, A. Roth, B. Sakmann, *J. Physiol.* **500**, 409 (1997).
18. W. Denk, J. H. Strickler, W. W. Webb, *Science* **248**, 73 (1990).
19. R. Yuste, A. Majewska, S. S. Cash, W. Denk, *J. Neurosci.* **19**, 1976 (1999).
20. T. G. Oertner, B. L. Sabatini, E. A. Nimchinsky, K. Svoboda, *Nat. Neurosci.* **5**, 657 (2002).
21. G. J. Stuart, H. U. Dodt, B. Sakmann, *Pflugers Arch.* **423**, 511 (1993).
22. Materials and methods are available as supporting material on *Science* Online.
23. L. Wu, P. Saggau, *Trends Neurosci.* **20**, 204 (1997).
24. J. Schiller, Y. Schiller, D. E. Clapham, *Nat. Neurosci.* **1**, 114 (1998).
25. D. M. Kullmann, *J. Neurosci. Methods* **30**, 231 (1989).
26. C. Stricker, S. Redman, D. Daley, *Biophys. J.* **67**, 532 (1994).
27. B. Cauli *et al.*, *Proc. Natl. Acad. Sci. U.S.A.* **97**, 6144 (2000).
28. F. Helmchen, K. Imoto, B. Sakmann, *Biophys. J.* **70**, 1069 (1996).
29. E. Neher, G. J. Augustine, *J. Physiol.* **450**, 273 (1992).

30. We thank B. Sakmann for his support during the early stages of this project and for critically reading the manuscript. Supported by the European Union and by NIH grant nos. NNS37444, MH48432, and MH44754.

Supporting Online Material
www.sciencemag.org/cgi/content/full/1100815/DC1
Material and Methods
Fig. S1
References and Notes

27 May 2004; accepted 10 February 2005
Published online 17 March 2005;
10.1126/science.1100815
Include this information when citing this paper.

Nicotinic Acid Limitation Regulates Silencing of *Candida* Adhesins During UTI

Renee Domergue,[1] Irene Castaño,[1]* Alejandro De Las Peñas,[1]* Margaret Zupancic,[1] Virginia Lockatell,[2] J. Richard Hebel,[3] David Johnson,[2,4] Brendan P. Cormack[1]†

The adherence of *Candida glabrata* to host cells is mediated, at least in part, by the *EPA* genes, a family of adhesins encoded at subtelomeric loci, where they are subject to transcriptional silencing. We show that normally silent *EPA* genes are expressed during murine urinary tract infection (UTI) and that the inducing signal is the limitation of nicotinic acid (NA), a precursor of nicotinamide adenine dinucleotide (NAD^+). *C. glabrata* is an NA auxotroph, and NA-induced *EPA* expression is likely the result of a reduction in NAD^+ availability for the NAD^+-dependent histone deacetylase Sir2p. The adaptation of *C. glabrata* to the host, therefore, involves a loss of metabolic capacity and exploitation of the resulting auxotrophy to signal a particular host environment.

In the United States, *Candida albicans* and *C. glabrata* are the primary and secondary causes of both bloodstream and mucosal candidiasis (*1*, *2*). *Candida* accounts for about 25% of all urinary tract infections (UTIs) related to indwelling catheters, with *C.*